Received 02 Sept 2020; | Revised 25 Sept 2020; | Accepted 26 Oct 2020

DOI: xxx/xxxx

FULL PAPER

A Piezo Smart-Braid Harvester and Damper for Multifunctional Fiber Reinforced Polymer Composites (FRPCs)

Seyedalireza Razavi[1*] | Lorenzo Iannucci[1] | Emile Smith Greenhalgh[1]

[1]Faculty of Engineering, Department of Aeronautics, Imperial College London, London, UK

Correspondence
*Seyedalireza Razavi
Email: S.razavi14@Imperial.ac.uk
Email: S.razavi14@Outlook.com

Present Address
Imperial College London,
South Kensington campus,
London SW7 2BU,
UK

The past decade has seen the rapid development of wearable electronics, wireless sensor networks (WSNs), and self-powered implantable sensors. However, these devices usually require a continuous source of power supply to operate safely and accurately while having the least reliance on conventional battery systems–due to the recharging/maintenance burdens of batteries. Vibration-based piezoelectric energy harvesting (PEH) from environment, man-made machinery, and human body movements seems to be a promising solution. Herein, the first integration of a piezoelectric poly(vinylidene fluoride) (PVDF) yarn-braid microgenerator into a fiber reinforced polymer composite (FRPC) structure is reported. It is demonstrated that the developed smart composite exhibits multifunctional performances, including simultaneous structural (with ≈10% increased Young's modulus), energy harvesting, and vibration damping (with a damping factor of 125%). The results show that an average output voltage of 3.6 V and a power density of 2.2 mW.cm^{-3} can be achieved at strains below 0.15%, under cyclic loading tests between 1 to 10 Hz. Moreover, noticeable improvements are made in the crystallinity percentage and β-phase content of as-received PVDF yarns by, respectively, ≈34% and ≈37%, as a result of the applied coreless radial and axial corona poling techniques in this work.

KEYWORDS:
piezoelectric energy harvesting, smart materials, multifunctional composites, poling, characterization

1 | INTRODUCTION

Rapid technological advances of internet of things (IoT), portable devices, wireless sensor networks (WSNs), and microelectromechanical systems (MEMS) in the past decade have fostered the development of a new form of sustainable energy sources for powering billions of such devices worldwide.[1–3] Furthermore, recent improvements in reducing the size and power consumption of microelectronic devices have inhibited the use of batteries in many of these applications (particularly in inaccessible areas) due to issues such as weight, bulkiness, limited energy density and life cycle, wiring burden, hazardous disposal, and regular charging and maintenance requirements.[4] Therefore, energy harvesting (EH) from ambient energy sources, which would be wasted otherwise, seems to be highly promising, as a supplementary method or substitute for batteries to power low-power microelectronic devices.[5,6]

In this regard, the three well-established harvesting mechanisms are electrostatic, electromagnetic, and piezoelectric transducers.[7] The power density of these mechanisms is theoretically comparable. However, manufacturing micro- and nanoscale (downsizing) electromagnetic generators is very challenging, and as for electrostatic mechanisms, they require

a bias voltage to operate. Therefore, piezoelectric harvesters can be argued to be the most viable and efficient mechanism investigated so far, owing to their unequivocal advantages such as ease of application, high voltage output, requiring no moving part, and being conformable to the current common monolithic MEMS manufacturing processes.[8–12]

However, recent increasing technological growth of wearable electronics, self-powered wireless sensors, and EH from human movements has urged researchers to explore new materials for the development of highly flexible piezoelectric transducers that could bear bending and twisting forces in real-life applications.[13–15]

This has shifted the research interest from the most popular ceramic-based piezoelectric materials, such as lead zirconate titanate (PZT) and barium titanate ($BaTiO_3$), to their polymer-based counterparts such as poly(vinylidene fluoride) (PVDF) and its copolymers poly(vinylidene fluoride-co trifluoroethylene) (PVDF-TrFE)).[16–18] This is because piezoceramics are inherently too brittle to be used in EH applications in the field of flexible devices and shaped geometries despite having excellent piezoelectric properties and a high energy conversion rate.[19,20]

Other flexible forms of PZT and $BaTiO_3$, including nanowires and nanofibers, are also too difficult to be mass-produced and scaled up.[8] PVDF and its copolymers, on contrary, are very flexible and can be formed into curved shapes whilst still remaining functional under large deformations. PVDF, particularly, has attracted much attention in recent years because of its unique advantages, including nontoxicity, excellent mechanical strength and stiffness, chemical inertness, high dielectric value, low moisture absorption, UV-light resistance, and low density.[21–24]

Moreover, when used in the fiber form, PVDF exhibits high sensitivity ($N.m^2$) to even small mechanical stimuli, such as rain and wind pressure, due to having a high aspect ratio (typically >1000:1) (A high aspect ratio (large surface area over a very small cross section) causes for even small longitudinal forces to create large stresses in the fiber.[25]

PVDF is a semi-crystalline polymer which has at least four different polymorphs: α, β, γ, and δ.[26] Among these, β phase is of particular significance, as it is the most thermodynamically stable phase in the material that contributes to the dielectric, piezoelectric, and ferroelectric properties of PVDF.[27–29] However, the overall paraelectric and ferroelectric properties of PVDF are governed by the relative parentage of each crystalline phase, which can vary depending on the processing condition. Nevertheless, one way to achieve the highest piezoelectric effect in PVDF is by increasing the β-phase content through mechanical stretching, as well as aligning the molecular dipole moments by the application of an external electrical poling process.[30]

Accordingly, over the past decade, the utilization of conventional hot-melt extrusion and spinning techniques (such as dry spinning, wet spinning, and electrospinning) has found extensive uses in the production of most 0D (filament) and 1D (yarn) piezoelectric PVDF fibers.[31]

This is because these techniques involve an application of large mechanical stretching ratios (3–5 times the original length) which is solely enough to enhance the piezoelectric properties of PVDF during crystallization from the melt without any further treatments (even up to a F(β) of 88.19%).[32] Consequently, the majority of the work concerning with the production of fibrous piezoelectric energy harvesters has focused on the use of melt-extruded and melt-spun PVDF fibers.[3,23]

In general, such harvesters are produced in the form of a core–shell structure, where the core is usually either a metal wire (e.g., Cu, Ag) or a conductive polymer yarn (e.g., carbon black/ polyethylene) that is simultaneously coextruded along with the sheath (PVDF). Also, the outer electrode in these structures is usually formed either by spiral-winding multiple bundles of conductive fibers around the core–sheath structure or via directly depositing a metallic layer (e.g., silver-paste, or gold-sputter) onto the outer surface of PVDF. Based on these configurations, meltspun PVDF fibers have been widely used for EH in the textile applications.[33–35]

The earliest account includes the work of Hadimani, in which a piezoelectric PVDF fiber was developed by a simultaneous hotmelt extrusion and an in-line high-voltage (13 kV) poling process. The fibers were sandwiched between two copper plates, and a maximum voltage output of 2.2 V was generated after impacting the structure with a weight of 1.02 kg from a height of 5 cm.[36,37]

In another study, a 2D piezoelectric PVDF force sensor was developed by utilizing the weaving process to intertwine melt-spun PVDF fibers into various weave architectures. It was shown that an impact force of 70 N upon a 1 Hz frequency could generate an average voltage of 3–4 V.[38]

Also, a 3D spacer piezoelectric textile energy harvester was developed by Soin et al.[26] It was demonstrated that a maximum voltage of 14 V can be generated under an impact pressure of 20–100 kPa by a knitted single-structure harvester, consisted of the melt-spun piezoelectric PVDF fibers woven with silver-coated polyamide-66 (PA66) conductive yarn electrodes. More recently, a washable co-axial woven piezoelectric generator was reported by Lund.[39] The device was constructed by weaving the conductive core electrode and the sheath PVDF layer in the warp direction, and the outer conductive electrode in the weft direction to prevent potential shorting. The generated output voltage of the device was measured to be about 3.5 V when a sinusoidal axial strain of 0.25 was applied at 4 Hz frequency.

Although the use of conventional melt-spinning techniques to produce fibrous PVDF harvesters has been well documented in the literature, there still exist several issues associated with the performance of melt-spun PVDF biocomponent fibers, which have been often overlooked in many studies, for example, poor fatigue performance, difficulty to achieve a uniform contact interface between the core–sheath components due to mismatches of their processing temperature, Young's modulus, and Poisson's ratio (consequently leading to thermal stress and weak adhesion problems),[40] and typical core-related issues due to mechanical stretching process, including breakage and discontinuities (in the case of using metal wires),[26] or a significant reduction in the electrical conductivity of the core due to a reduction in the cross-sectional area of the fiber (in the case of using conductive polymers).[41]

To overcome these issues, we reported, for the first time,[42,43] on the concept of utilizing the braiding technology to fabricate a novel all-fiber piezoelectric PVDF smart-braid microgenerator. Based on the same concept,[44] in this work also, we have developed an industrially scalable piezoelectric PVDF smart-braid microgenerator, which consists of 24 piezoelectric PVDF yarns that are braided, respectively, over and under a solid core copper wire inner electrode, and 16 strands of braided copper wires outer electrode.

Furthermore, to the best of our knowledge, no previous study has yet investigated the possibility to incorporate such a smart microgenerator within a fiber reinforced polymer composite (FRPC) structure.[45] Therefore, this work will generate fresh insight into the development of a new class of smart FRPC structures with multifunctional performance capabilities, including simultaneous load-bearing, sensing/EH, and vibration damping, with potential uses in the automotive and aerospace sectors.

2 | EXPERIMENTAL SECTION

2.1 | Materials

Lenzing Lenofil PVDF multifilament yarns were purchased from Lenzing Plastics (Austria).[46] Each yarn, constituted of 48 filaments, had an average diameter of 0.16 mm and a linear density of 150 dtex (dtex = weight in grams per 10 000 m of continuous filament yarns).

To explore the effect of utilizing different types of core electrodes on the mechanical properties of the final harvester, four types of commercial conductive yarns were purchased: a copper-cladded zylon fiber core (0.24 mm/146 tex) from Syscom Advanced Materials, USA (Amberstrand166),[47] a copper-cladded vectran fiber core (0.22 mm/108 tex) from Syscom Advanced Materials, USA (Liberator40),[48] a plasma metal (silver)-coated polyamide (PA66) yarn core (0.17 mm/17 tex) from Swicofil, Switzerland,[49] and a polyurethane (PUR)-enamelled copper wire core (0.4 mm/1450 tex) from RS Components, UK(RS No. 337-7050).[50]

The latter type was also purchased in a diameter of 0.1 mm/88 tex (RS No. 337-7088) so as to be used for the outer electrode layer of all harvesters (Figure S1 and Table S1, Supporting Information). To only account for the true cross sections and diameters of yarns (excluding air gaps between filaments), linear density (g m^{-1}) of samples was measured experimentally and divided by their densities (gr.m^{-3})–following ASTM D1577.[51]

2.2 | Fabrication of Hybrid Braid Microgenerators

Prior to fabricating samples of piezoelectric PVDF microgenerators, all yarns were transferred from their as-received bobbins to smaller bobbins (using a Herzog Eltra USP300 filament-winding equipment), to match the size of the rotary carriers on the braiding machine (**Figure** 1 a).

Next, a Maypole braiding machine (Herzog RU 2/16-80 A) was used to fabricate four types of hybrid braids (Figure 1 b), incorporating eight PVDF yarns braided over different conductive core electrodes (see further on the fabrication process in Figure S2, Supporting Information).

The fabricated samples included a PVDF/Cu-coated zylone core, a PVDF/Cu-coated vectran core, a PVDF/Ag-coated PA66 core, and a PVDF/PUR-enamelled Cu core (Figure 1 c). Finally, all samples were overbraided with 16 strands of a 0.1 mm PUR-enamelled Cu wire to form the outer electrode layer of microgenerators (Figure 1 d).

2.3 | Tensile Test

Complying with the ASTM standard D2256,[52] a single-strand method was adopted to determine the mechanical properties of the fabricated hybrid braids under a series of tensile tests.

To avoid issues associated with testing fibrous samples, such as slippage, damage due to the clamping force, and even jaw breaks, a set of pneumatic yarn grips (Instron 2714-005 Series) were used to clamp all fibrous samples on a universal testing machine (5960 Series Instron)–following the test procedure described in ASTM D7269.[53]

All samples had a gauge length of 150 ± 1 mm, and the tests were performed at a constant cross-head speed of 1 m.min^{-1}, corresponding to a quasi-static strain rate of 0.01 s^{-1}.

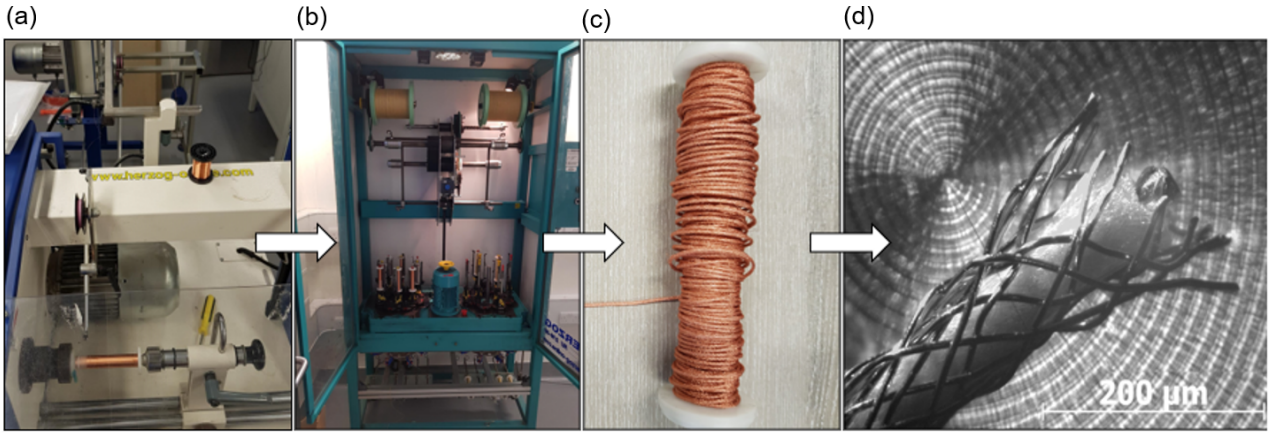

FIGURE 1 The manufacture of piezoelectric smart hybrid braids: a) filament winding equipment; b) Maypole braiding machine equipped with two rotary heads, each head having eight horn gears and eight carriers; c) a representative sample of the fabricated smart hybrid braid prototypes; and d) a microscopic image of the developed piezoelectric smart-braid harvester composed of a core electrode (a 0.4 mm PUR-enamelled copper wire), a piezoelectric sheath (8 PVDF yarns), and an outer electrode layer (16 strands of a 0.1 mm PUR-enamelled Cu-wire).

2.4 | Poling

To enhance the piezoelectric properties of as-received PVDF yarns, two poling approaches were investigated: a contactless radial and a coreless axial poling method.

2.4.1 | *Radial Poling*

A custom-designed radial poling apparatus, composed of a set of spur gears and parallel copper plate electrodes (being 2 mm apart), was used to simultaneously stretch and corona pole (SSCP) PVDF yarns along the radial (thickness) direction of fibers (Figure S3, Supporting Information).

In this method, two approaches were examined: 1) poling under a constant voltage (1 kV) but at different exposure times (10–60 min); 2) poling under a constant exposure time (1 min) but under different poling voltages (1–4.9 kV).

2.4.2 | *Axial Poling*

In this method, a DC high-voltage potential of 55 kV was applied along the axial direction of a 100 mm-long PVDF yarn bundle, which was connected directly to the ground and positive port of a high-voltage power supply unit (Figure S4, Supporting Information). The poling voltage was increased stepwise from 0 to 55 kV, using two different rates: 1 kV.s^{-1} and 1 kV.min^{-1}.

The maximum voltages of 4.9 and 55 kV were the respective corona voltage thresholds found during the radial and axial poling experiments based on the distance between electrodes of the poling equipments and the environmental conditions (an average relative humidity of 55% and a temperature of 18°C).

2.5 | Characterization

Similar to the work performed in previous studies,[54,55] differential scanning calorimetry (DSC) and Fourier transform infrared (FTIR) spectroscopy characterization techniques were carried out to obtain information regarding the degree of crystallinity and the β-phase fraction of PVDF. Here, DSC was used as a complementary technique to the FTIR spectroscopy, as DSC does not distinguish the crystalline phases of PVDF (α, β, γ, and λ).[55,56]

In general, it is expected from the DSC thermograms that an improvement in the crystal structure of PVDF manifests as a reduction in the melting temperature of sample from 172–175 °C (α-phase range) to 165–172 °C (β-phase range) (the lower melting temperature of the β-phase as compared with the α-phase is because the latter is entropically more stable[57]), and/or as an increase in the overall crystallinity (X_c) of the material.[58,59] Accordingly, the percent crystallinity (%) can be quantified by measuring the enthalpy of melt ΔH_m of the sample divided by the enthalpy of melt ΔH_m^0 of fully crystalline PVDF (104.6 J.g^{-1})[60] using Equation (1).

$$X_c = \Delta H_f(T_m)/\Delta H_f^o(T_m^o) \quad (1)$$

Similarly, from the FTIR spectra, an α- to β-phase transformation is expected to be observed as an increase in intensities of the intrinsic β-phase absorption peaks, and/or through a noticeable shift in the as-produced offset β-phase peaks toward the characteristics ("fingerprint") peaks at 840, 1275, and 1401 cm^{-1}.[61]

Accordingly, the relative β-phase ratio in samples can be identified from the following Equation (2).

$$F(\beta) = \frac{A_\beta}{1.26A_\alpha + A_\beta} \quad (2)$$

where, A_α and A_β are the absorbance band intensities corresponding to the wave numbers at 763 and 840 cm^{-1}, respectively.

In this work, a DSC analyzer (Discovery DSC1-0438/TA Instrument) was used to study changes in the melting temperature (T_m), and improvement in the degree of crystallinity (X_c) of samples. The procedure was carried out at a constant heating rate of 10 °C.min^{-1} on an average sample weight of ≈5 mg, and under a nitrogen atmosphere in a temperate ranging from –40 to 250 °C.min^{-1}. The types of samples used included the following: as-received PVDF yarn, a commercial piezo spiral wrapped coaxial cable (purchased from *Measurements Specialties*),[62] and the radially and axially samples poled in this work.

Verification on the phase transformation of the poled samples was made via FTIR spectroscopy analysis, using a Perking Elmer spectrometer. The FTIR spectra were obtained in the attenuated total reflectance (ATR) mode, and in the wave number ranging from 450 to 4000 cm^{-1}. However, here only the range between 600 and 1500 cm^{-1} was investigated as the major PVDF crystal phases occur in this region.

2.6 | Fabrication of Smart Composite Structures

The developed piezoelectric smart-braid microgenerator was embedded within a number of glass fiber reinforced polymer (GFRP) composite panels, which were made using a resin infusion under flexible tooling (RIFT) process (see the fabrication process in Figure S5 and S6, Supporting Information). Such smart composites have a multifunctional capability, including simultaneous structural (load-bearing), sensing, EH, and vibration damping. **Figure** 2 represents one example of the as-produced smart composite panel fabricated in this work.

The reinforcement material used was dry S2-glass (Sigmatex) biaxial [(0/90)] noncrimp fabrics (NCF), having a density of 2.238 ± 0.04% gr.cm^{-3}, and the matrix part was prepared from a mixture of a 100%*wt* low-cure resin epoxy (Prime™20 LV) and a 26%*wt* slow hardener (Prime™20). The cure temperature of the resin system was around 50 °C, which is well below the optimum operating temperature of PVDF (≈77°C above which the piezoelectricity of PVDF starts degrading).[63]

The layup consisted of eight layers ($[(0/90)_{4s}]$), and the smart braid harvester was embedded during the hand layup process between the second and third layers of the NCF blankets. After consolidation, five rectangular specimens with dimensions of 400 mm × 60 mm were water jet cut and prepared for the EH experiments (see other fabricated concept prototypes in Figure S7, Supporting Information).

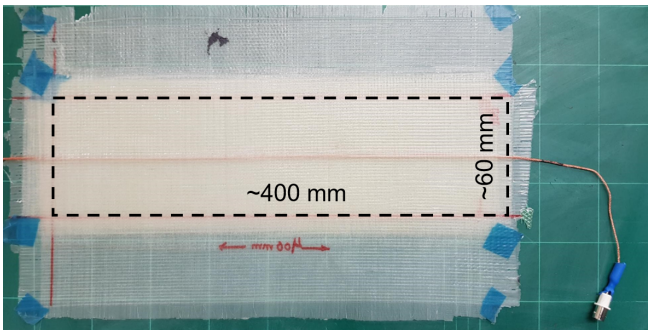

FIGURE 2 Fabricated smart GFRP composite panel before water jet cutting.

2.7 | EH Experiments

The manufactured smart composite specimens were subjected to a series of three-point bending (3PB) cyclic loading tests after fabrication. A servohydraulic Instron fatigue machine was used to apply 2 mm-displacement-controlled harmonic excitation forces in a frequency range of 1–10 Hz (**Figure** 3 a).

For this aim, a custom designed 3PB fixture was used to hold the specimen in the free-free boundary condition. To eliminate the possibility of double impacts during loading-unloading cycles, the third (loading) cylinder was carefully lowered down to slightly touch the upper surface of specimen prior to starting the experiments–applying a small preload of <5 N.

Based on an average specimen thickness of 2.4 mm, a support span of 145 mm was defined between the fixture supports to comply with the minimum support span-to-thickness ratio of 60:1, described in ASTM D7264.[64] An average length of the embedded smart-braid within composite was ≈400 mm, with an extra ≈50 mm being extended outside for wiring purposes.

As shown in Figure 3 b, the piezo-generated charges were first converted into voltage signals via a piezo lab amplifier (purchased from the *Measurements Specialties*).[65] Voltage signals were then sent simultaneously to a data acquisition unit (NI compact USB-6229)–to output VAC, and to an AC-to-DC rectifier circuit–to output VDC, IDC, and PDC (Figure 3 c).

The rectifying circuit, which consists of a 4-pin diodes (2 A, 600 V from RS Components: 751-4464), a 470 μF shunt capacitor (from RS Components: 711-1110), and two separate shunt resistors (1 and 100 kΩ), served also as a mechanical damping mechanism to waste the extracted electricity as heat over the shunt resistors (Figure S8, Supporting Information).

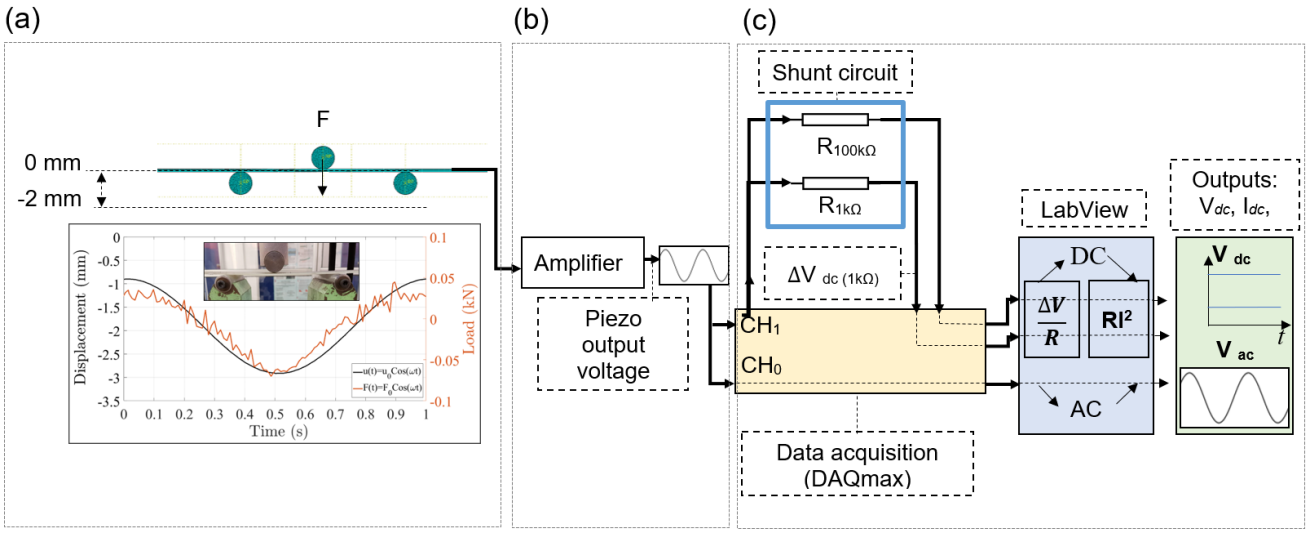

FIGURE 3 Schematic of the EH process under cyclic loading tests: a) the experimental setup of a smart composite prototype in a 3PB configuration (the mechanical part); b) the generated piezo-charges being converted to AC voltage signals (the mechanical-electrical part); and c) the AC-to-DC signals conversion via 1 and 100 kΩ full-bridge rectifying circuits (the electrical part).

2.8 | Damping

Experimental modal analysis on a smart GFRP composite specimen was performed to investigate the damping performance of the embedded smart-braid microgenerator as a passive-damping device. A cantilever beam specimen with dimensions of 400 mm × 60 mm × 2.4 mm was used to perform the free-vibration tests.

As shown in **Figure** 4 , one end of specimen was tightly fixed between two flat steel grips, while the other end was freely excited by hand. During the tests, a piezoelectric accelerometer (Measurement Specialities ACH-01) and a signal acquisition card (NI USB 6223; data acquisition DAQmax) with LabView program were used to record the vibration responses.

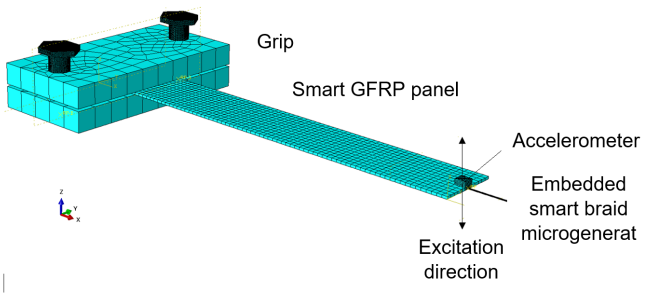

FIGURE 4 A demonstration of the experimental setup used for vibration damping analysis of the manufactured smart composite panels.

3 | RESULTS AND DISCUSSION

3.1 | Tensile Test of Hybrid Braids

Figure 5 shows the results of the tensile tests and electrical conductivity measurements of the fabricated hybrid braids using the 4-wire resistance test method.

As the bar charts show, PVDF/PA66 braid (hybrid braid A) exhibited both the lowest Young's modulus (747 MPa) and the core electrical conductivity (0.08×10^6 S/m), as compared with other sample types. Consequently, this braid was excluded from further analysis in this work. The elastic moduli of all

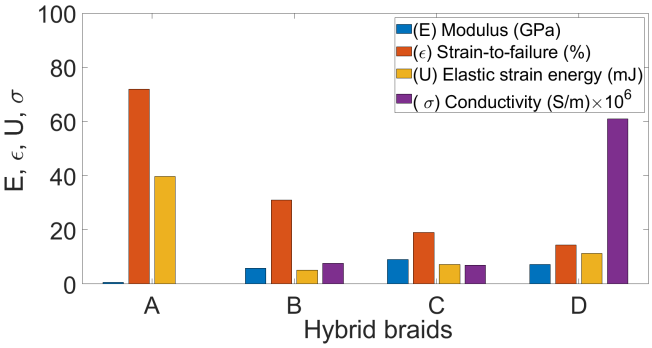

FIGURE 5 The mechanical and electrical properties of the fabricated hybrid braids. Eight PVDF yarns braided over a core Ag-coated PA66 fiber in A, a core Cu-coated vectran fiber in B, a core Cu-coated zylon fiber in C, and a core PUR-enamelled Cu wire in D.

other braids (B, C, and D), however, were reasonably high and in the same orders of magnitude ranging from 6 to 9 GPa.

In terms of the strain-to-failure, these values for hybrid braids B and C were found to be, respectively, ≈53% and ≈24% higher than that of braid D. This is most likely due to the superior mechanical properties of the incorporated high-strength zylon (Amberstrand) and vectran (Liberator) core fibers used in these braids, compared with those of the PUR-enamelled Cu wire core electrode utilized in braid D.

However, it is worth noting that a higher value of strain-to-failure may not necessarily reflect a fair comparison of the expression of the piezoelectric performance of different transducers; as all piezoelectric energy harvesting (PEH) devices are designed with the intention to operate only within the elastic region of their constituent materials, rather than to structurally fail under large strains.

On the contrary, the elastic strain energy can be said to be a better metric for determining the extent to which the applied mechanical energy (i.e., the elastic strain energy) can be absorbed by a PEH device without experiencing a plastic deformation. As can be seen from Figure 5 , the elastic stain energy for hybrid braid D is, respectively, about 54% and 34% higher than the corresponding values obtained for braids B and C–in addition to having a core conductivity in the order of 6–7 times higher than the latter types. For these reasons, hybrid braid D (PVDF/PUR-enamelled copper core) was chosen over other types for further development of a PVDF smart-braid harvester in this work.

3.2 | Piezoelectric Performance Optimization

To assess the influence of PVDF yarns on the mechanical properties and, consequently, on the piezoelectric performance of hybrid braid D (fabricated in Section 3.1), two other variations of this braid were made; this was done by repeating the overbraiding process twice to add eight PVDF yarns during each run.

Thus, the final number of PVDF yarns was increased from 8 to 16, and finally, to 24 yarns, as shown in **Figure** 6 a) i, b) i, and c) i, respectively. Figure 6 a) ii, b) ii, and c) ii also show the corresponding scanning electron microscopy (SEM) morphologies of these preforms after being overbraided with 16 strands of a 0.1 mm PUR-enamelled Cu wire outer electrode.

Due to the unique advantages of braiding technology (repeatability, reproducibility, and cost-effectiveness), the overbraiding processes were performed without requiring complex adjustments of the fabrication process. In addition, no modification was done to the braiding parameters, e.g., the take-up speed and the braid angle, as well as the constituent materials including the inner and outer electrodes.

Figure 7 shows the tensile test results of these samples. It is apparent from this figure that braiding technology has provided an effective way of improving the mechanical properties of the fabricated traixal performs while using the same core electrode in all braids (because core is the main load-bearing constituent part in triaxial preforms).[66] Surprisingly, it is interesting to note that the load-bearing capability of the core itself was

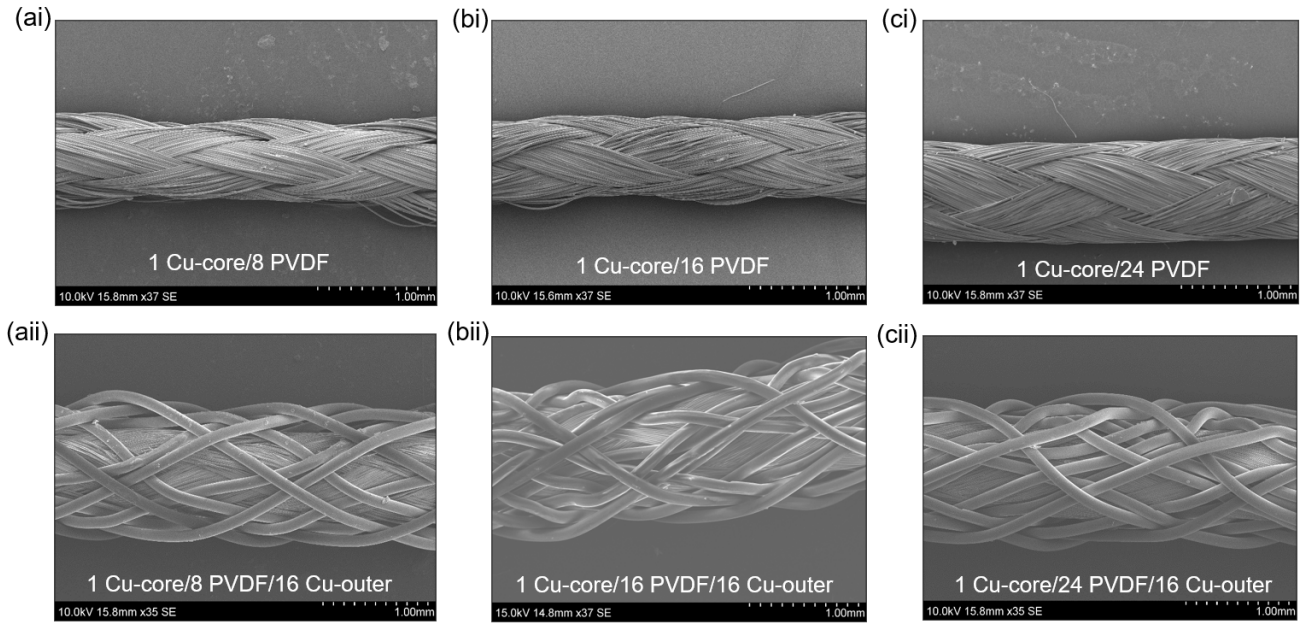

FIGURE 6 SEM images of three variations of piezoelectric PVDF smart-braid fabricate during separate overbraiding processes. A 0.4 mm PUR-enamelled Cu wire core electrode overbraided with a) i 8, b) i 16, and c) i 24 PVDF yarns. All preforms subsequently overbraided with 16 strands of a 0.1 mm PUR-enamelled Cu wire outer electrode in a) ii, b) ii, and c) ii.

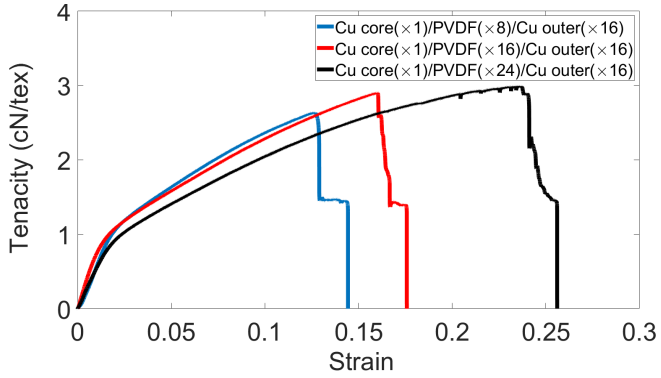

FIGURE 7 Stress versus strain curves of the fabricated three variations of hybrid braid D.

improved as a result of increasing the number of circumferential PVDF yarns. For instance, the elongation-to-break and ultimate tensile strength were increased by ≈75% and ≈13%, respectively (Figure S9a, b, Supporting Information).

The results, therefore, suggest a strong dependence of the mechanical properties of the fabricated smart-braid on the number of intermediate PVDF yarns. In other words, the piezoelectric performance of harvester can be directly enhanced by improving the mechanical properties of the preform as a result of adding more PVDF yarns to the structure.

This further signifies the key advantage of braiding technology compared with the conventional melt-spinning process, in terms of the adaptability of the braiding process to manipulate the piezoelectric response of harvester, such that to meet the final EH requirements of a particular application of interest.

3.3 | EH of Smart Composite Structure

The EH performance of the developed piezoelectric smart-braid was investigated as an embedded microgenerator in a GFRP composite panel (Section 2.7, Figure 2). **Figure** 8 a, b shows the generated voltage outputs of the microgenerator as a function of cyclic excitation forces. The results are also shown in Table 1 . As shown in Figure S10 and S11 (Supporting Information), the generated voltage signals show a frequency dependence and follow the sinusoidal waveform as that of the applied forces. The results presented here (Figure 8 a, b), however, are only the final rectified signals (V_{dc}) under a 1 kΩ and a 100 kΩ shunt resistor.

From the voltage versus load curves in Figure 8 , it is apparent that the magnitudes of the applied load increased in a relatively linear fashion as the excitation frequency increased (explained by the relationship between force, angular velocity, and frequency ($F = m\omega^2 r$)). Similarly, the generated voltage outputs under a 100 kΩ resistor (Figure 8 b) increased with frequency, reaching its peak (≈3.8 V) at around 3 Hz, and

TABLE 1 The generated voltage outputs of the embedded smart-braid harvester within a GFRP composite structure.

Frequency [Hz]	Force [N]	Voltage [V]	
–	–	1 kΩ	100 kΩ
1	29.7	3.85	3.02
2	30.7	4.16	3.31
3	31.4	4.14	3.35
4	32.1	4.11	3.34
5	33.5	3.99	3.31
6	34.1	3.96	3.32
7	35.1	3.94	3.33
8	37.8	3.92	3.31
9	43.8	3.9	3.29
10	46.3	3.85	3.28

remained relatively steady afterward around an average voltage of ≈3.2 V up to 10 Hz.

As for the 1 kΩ system, however, a different behavior was observed (Figure 8 a), where after 2 Hz, at which the peak voltage occurred, there was first a gradual and then a sharp fall in the magnitudes of the output V_{dc}, from ≈4.15 to ≈3.85 V. This drop could be explained by the fact that using a small load resistor resulted in the time constant (RC) to be relatively small, and therefore the rate of discharge of capacitor through the resistor was faster than the source (piezoelectric smart-braid) charging period.

On the contrary, using a higher value of shunt resistance (100 kΩ) was advantageous in terms of increasing the time constant (RC), and thus helping to minimize the rate of discharge of capacitor at higher frequencies. As a consequence, the generated voltage signals were found to be more stable (less fluctuating) in this case. The results of voltage and power outputs of other smart composite concept prototypes are shown in Figure S12–S16, Supporting Information.

Nevertheless, it is worth noting that despite the fact that more fluctuations were observed in the output signals of the 1 kΩ resistor, the lowest rectified voltage output of this system (around at 1 Hz) was still ≈15% higher than that of the corresponding maximum voltage output obtained by its 100 kΩ counterpart (around at 2 Hz).

In other words, the latter system induced a higher damping effect by consuming ≈15% of the stored energy within the parallel capacitor in the rectifier circuit. Although this may not be advantageous from the EH point of view, it is very desirable in terms of the mechanical damping performance. Therefore, selecting the right shunt–Ω value plays a key role in achieving an optimum trade off between the voltage output and the mechanical damping effect in such multifunctional structures.

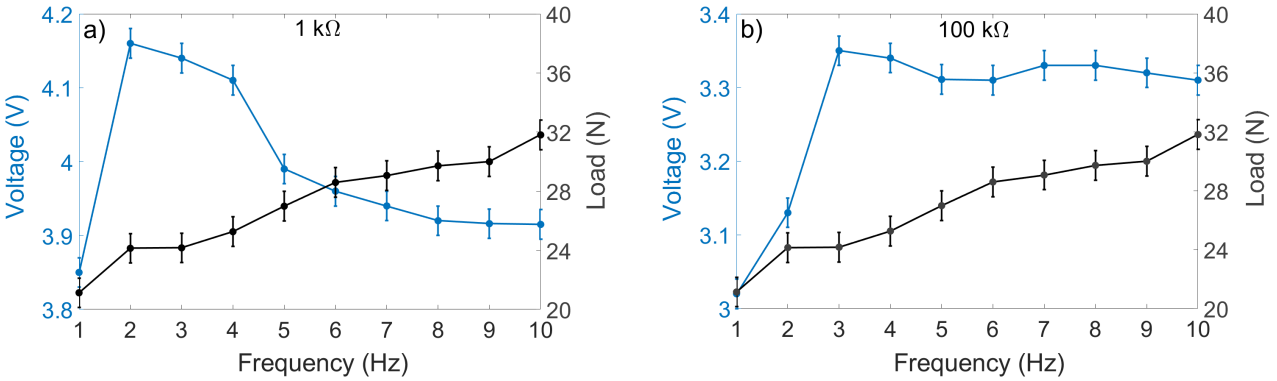

FIGURE 8 The generated output voltages at different excitation frequencies over a) a 1 kΩ, and b) a 100 kΩ shunt resistor.

A similar phenomenon confirming a higher induced damping effect caused by a higher resistive load (R_L), was also observed from the results of the free-free vibration tests, as shown in **Figure** 9 .

As can be seen from Figure 9 a–c, the vibration amplitudes decayed exponentially due to the effect of introducing a high R_L to the system. To quantify this decay, the logarithmic decrement (δ) of the first and 20th vibration amplitudes were calculated using Equation 3 and 4. Subsequently, the results reveal that the damping ratio (ζ) increased nearly sevenfold, from ≈1.83%, in the case of an open circuit (OFF-mode), to ≈12.31%, in the case of the 1 kΩ resistor, and finally, to ≈12.64%, in the case of the 100 kΩ resistor.

$$\delta = \frac{1}{20} ln \frac{X_{p-p}}{X_{p-p(20)}} \tag{3}$$

$$\zeta = \frac{\delta}{\sqrt{4\pi^2 + \delta^2}} \tag{4}$$

where X_{p-p} and $X_{p-p(20)}$ are the respective peak–peak vibration amplitudes during the first and 20th cycles. It is, therefore, safe to conclude that increasing the value of R_L would yield in more dissipation of the harvested energy as heat, therefore inducing a higher damping effect into the system.

However, at very high loads, a complete opposite effect can happen, where a further increase in the R_L value would no longer result in an increase in the damping effect–as reported also in the previous studies.[67,68]

Therefore, to develop a full picture of the damping behavior of the developed smart-braid harvester, additional studies will be needed to experimentally establish an optimum relationship between the maximum value of R_L and the maximum damping effect (ζ) that can be achieved under a particular range of excitation frequencies.

3.4 | Tensile Performance of Smart Composite

Apart from the simultaneous EH and mechanical damping capabilities of the developed smart composite, the third functionality to assess was in terms of the structural (load-bearing) performance. For this aim, at least five smart- and five plain-type GFRP specimens were subjected to a series of tensile tests–following the standard ASTM D3039 procedure.[69]

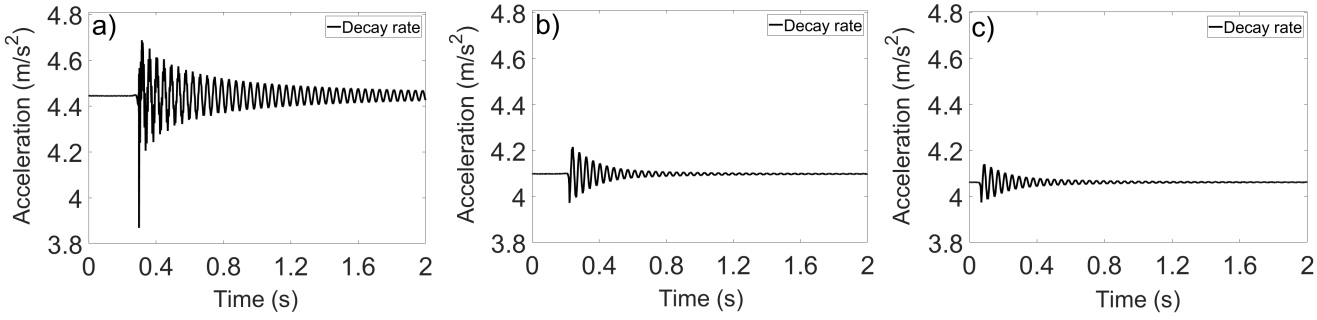

FIGURE 9 The mechanical damping performance of the embedded smart-braid harvester within a GFRP composite panel. a) When harvester is not operating (an open circuit), and when harvester is operating through the rectifying circuits under b) a 1 kΩ and c) a 100 kΩ shunt resistor.

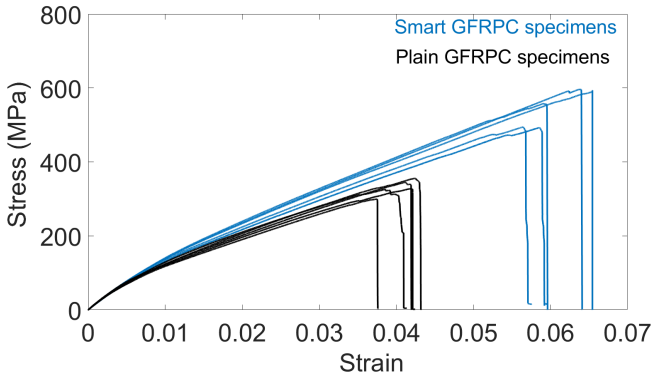

FIGURE 10 Comparison of the tensile properties of the fabricated plain and smart–type composite panels.

As can be seen from **Figure** 10 , the tensile test results reveal that a noticeable improvement was made within the tensile properties of the smart-type specimens, where the ultimate tensile strength, Young's modulus, strain-to-failure, and strain energy of the panels were increased, respectively, by ≈40%, ≈10%, and ≈35%, as compared to the plain-type counterparts.

3.5 | Material Characterization

3.5.1 | *DSC*

The DSC thermograms of the axially and radially poled yarns, as-received PVDF, and a commercial type of PVDF-film (spirally wrapped strips)[62] samples are shown in **Figure** 11 . A summary of the crystallinity % of samples is also shown in Table 2 .

As can be seen in Figure 11 a–c, the first positive sign regarding the enhancement of the crystallinity level of the poled yarns is manifested as a reduction in the average melting temperature of samples, which is from 172.82 °C (in the as-received yarns) to 171.5 °C (in the poled yarns).

Consistent with the literature,[70,71] such an effect indicates the initiation of a permanent piezoelectric effect due to the application of high-voltage poling treatments performed in this work.

Another important feature regarding the α to β-phase transition in the poled samples can be seen (in Figure 11) as changes in the shapes of the melting peaks from broad endothermic (double) in the as-received yarns to sharper single peaks in the poled yarns, with the intensity of peaks increased. The sharper melting peaks are representative of the formation of more β-phase fractions within the material, implying that there is a less broader distribution of crystalline domain size within the polymer.[57]

Furthermore, the data in Table 2 confirm that the crystallinity percentage (X_c) of the as-received PVDF were improved both in the radially and axially poled yarns. For instance, in the former, this improvement was about 7–23% and 6–30% for the yarns poled under a constant exposure time (1 min) and under a constant poling voltage (4.9 kV), respectively; in the latter, this was about 31% and 34% for the samples poled under the slowest (1 kV.min^{-1}) and the fastest poling rates (1 kV.s^{-1}), respectively.

TABLE 2 The results of X_c (%) of PVDF yarn samples.

PVDF Samples	Poling [*V* / *t* / *rate*]	ΔH_m [J.g^{-1}]	T_m [°C]	X_c [%]
As-received	–	46.3	172.8	44.3
Commercial[(a)]	–	65.2	166	62
Radially poled *t*-constant (for 1 min)	1 kV	49.6	172.7	47.4
	2 kV	51.4	171.8	49.1
	3 kV	51.7	171.7	49.4
	4 kV	52.6	171.7	50.2
	4.9 kV	57.2	171.6	54.7
Radially poled *V*-constant (at 4.9 kV)	10 min	49.7	172.14	46.9
	20 min	53.9	171.8	51.5
	30 min	57.3	171.7	54.7
	40 min	58.4	171.7	55.8
	50 min	59.8	171.7	57.2
	60 min	60.6	171.6	57.9
Axially poled 0–55 kV	1kV.min^{-1}	61.1	169.5	58.2
	1kV.s^{-1}	62.3	168.9	59.5

[(a)] A piezoelectric PVDF coaxial cable formed of spirally wrapped PVDF thin strips (*Measurement Specialties*)[62]

3.5.2 | *FTIR*

The FTIR spectra provide information regarding the phase fractions and crystal structures of polymer, which help in distinguishing between different characteristic α, β, and γ phases of PVDF. Herein, the FTIR spectra of as-received PVDF and axially poled yarns were carried out to investigate the influence of the poling exposure time on the enhancement of PVDF β-phase content.

An initial comparison of the graphs (**Figure** 12 a) suggests that the nonpolar α and the polar β and γ phases (responsible for the piezo and pyro electric properties) coexist in both treated and untreated samples.

However, this was expected; as many previous studies[72–74] have shown that typically melt-spun PVDF fibers contain a noticeable amount of β-phase content solely because of the mechanical stretching process that is applied during the extrusion process. As a result, the exclusive peaks around at 614, 763, 795, 975, 1149, 1209, 1383, and 1423 cm^{-1}, with specific valleys around at 855 and 1423 cm^{-1}, are the representative

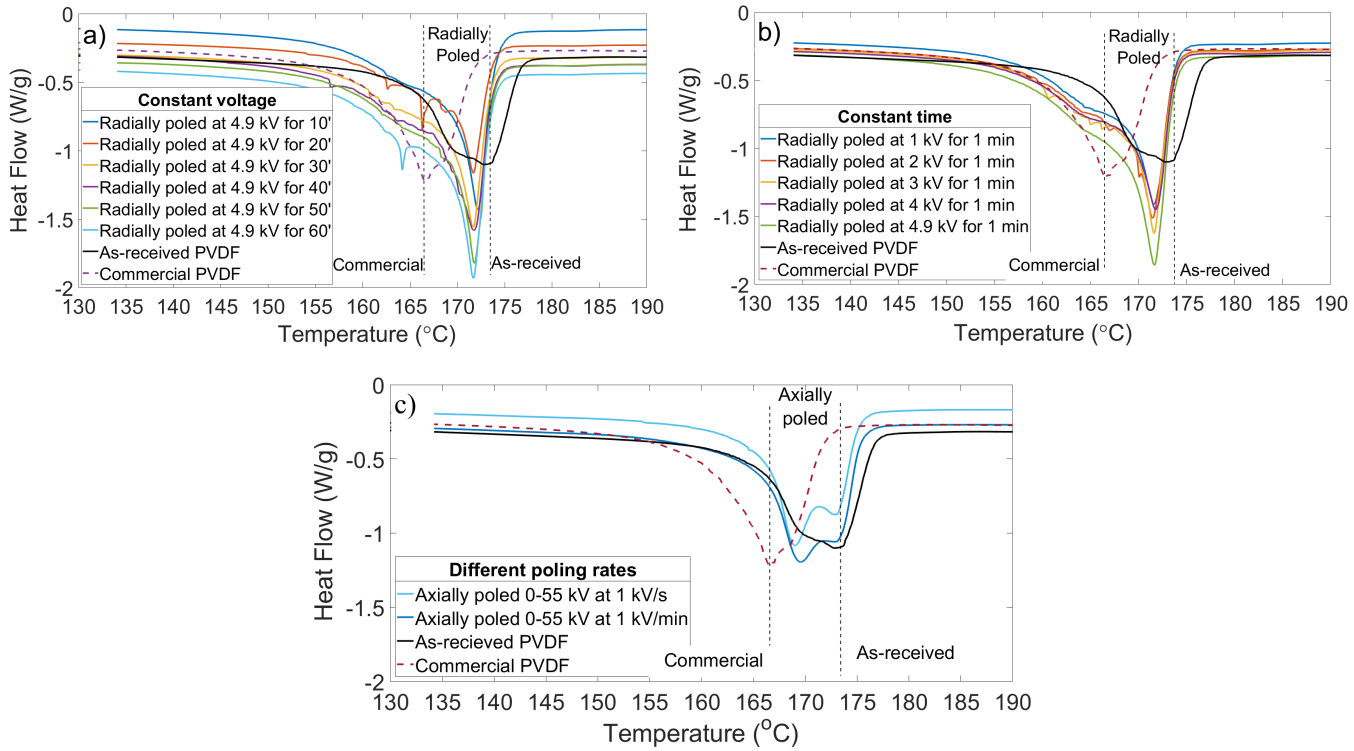

FIGURE 11 Comparison of the DSC thermograms of PVDF yarn samples. a) Radially poled yarns under a constant poling voltage; b) radially poled yarns under a constant exposure time; and c) axially poled yarns at two different poling rates.

characteristic absorption bands of the α-phase; exclusive wave numbers around at 445, 473, 840, 881, 1071, 1176, 1275, 1234, 1401, and 1431 cm^{-1} are attributed to those of the β-phase; and the exclusive γ peaks are those around at 431, 482, 838, 776, 1234, and 1429 cm^{-1}, with the two β peaks at 840 and 1431 cm^{-1} overlapping with those of the γ-phase at 838 and 1429 cm^{-1}.[61]

From Figure 12 a, it is observed that at low poling voltage ranges (<40 kV), there was no significant change in the β-phase peak intensities of PVDF. However, at higher voltages, near the corona discharge threshold (50 kV), such intensities increased, particularly, the characteristic β-phase bands at 840 and 1170 cm^{-1}; finally, upon reaching the maximum corona poling voltage of 55 kV, the intensities reached their maxima.

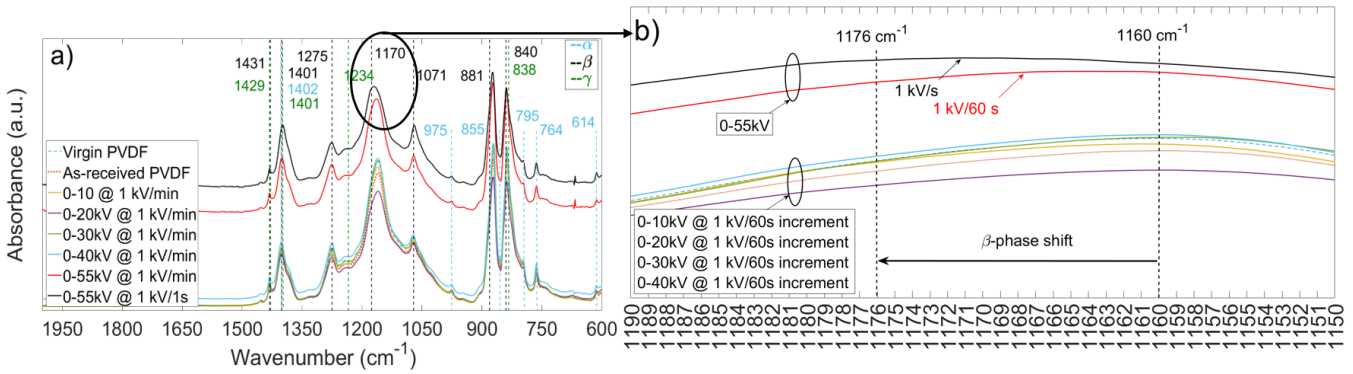

FIGURE 12 FTIR transmittance spectra for PVDF yarn samples. a) The coexistence of PVDF's characteristic absorption bands; b) an enlarge view showing the IR intensities of the fast-rate poled samples with a significant phase shift from 1160 cm^{-1} toward the fingerprint β-phase peak at 1176 cm^{-1}.

Particularly, the peaks at 614, 764, and 975 cm^{-1} (characteristics of α-phase) becoming weaker and exclusive peaks at 840 and 1071 cm^{-1} (characteristics of β-phase) became sharper and stronger (**Figure** 13).

One interesting finding is that at the corona voltage threshold (55 kV), where the poling voltage could not be increased any more, it was possible to improve the β-phase fractions of samples even further by means of increasing the poling rate (i.e., the voltage increments) from 1 kV min^{-1} to 1 kV s^{-1}. The positive influence of increasing poling rate on the improvement of PVDF's β- content can be also evident from Figure 12 b, where a clear shift has been taken place in the off-set β-phase peak band at 1160 cm^{-1} toward the fingerprint β-phase peak at 1176 cm^{-1}, in the yarns which were poled under the fastest poling rate. Note that the DSC test results also showed a similar effect, where the highest crystallinity % was developed within the samples which were poled by the fastest poling rate between 0 and 55 kV. These results imply a good agreement between the FTIR spectra and the DSC test results.

Accordingly, the β-phase fractions (Fβ) of yarns were calculated using Equation (2), and the results are presented graphically in Figure 13 . These values are 0.54, 0.58, 0.61, 0.65, 0.7, 0.72, and 0.74 for fibers poled between 0–10 (at 1 kV min^{-1} increment), 0–20 (at 1 kV min^{-1} increment), 0–30 (at 1 kV min^{-1} increment), 0–40 (at 1 kV.min^{-1} increment), 0–55 (at 1 kV.min^{-1} increment), and 0–55 (at 1 kV.s^{-1} increment), respectively. Overall, the DSC and FTIR analyses confirmed that there has been a noticeable improvement in the crystallinity % and β-phase fractions of the radially and axially poled samples. It was also revealed that the poling voltage has a direct influence on the enhancement of the piezoelectric properties of the yarns. However, a comparison of the melting temperature of samples in Table 2 suggests that the highest amount of permanent polarization effect has been induced mainly within the axially poled samples because of showing a higher reduction in their melting temperature (≈3.85 °C) compared with the radially poled yarns. In addition, a small difference (≈0.12 °C) observed between the T_m reduced in the radially poled samples (≈1.8 °C in the t-constant samples and≈1.2 °C in the V-constant samples) revealed that the crystallinity level of PVDF has been relatively independent of the exposure time factor, which is in agreement with the results reported elsewhere.[75]

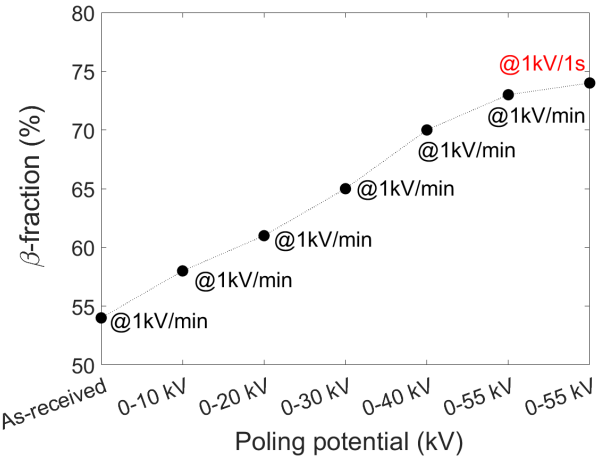

FIGURE 13 Comparison of the β-phase fractions developed within the axially poled PVDF.

4 | CONCLUSION

A novel all-fiber piezoelectric PVDF smart-braid harvester was developed by using low-cost and scalable textile braiding technology. Among the fabricated types of PVDF/core hybrid braids, the type equipped with a 0.4 mm PUR-enamelled Cu wire core electrode was found to be the most promising candidate harvester, showing good mechanical and electrical properties combined. It was also found that there is a strong dependency of the mechanical properties of the fabricated braid on the number of incorporated piezoelectric PVDF yarns, such that, for instance, by tripling the number of braided PVDF yarns from 8 to 24, the overall mechanical properties of the whole preform were improved noticeably, such as the elongation-to-break (by ≈75%), ultimate tensile strength (by ≈13%), and elastic strain energy (by ≈36%).

Furthermore, the piezoelectric performance of the developed harvester was investigated as an embedded microgenerator within a FRPC structure under cyclic loading tests between 1 and 10 Hz.

This research study yielded several promising findings, showing that the developed smart-braid exhibits 1) excellent chemical stability: as no insulating layer was used either around the electrodes, or at the PVDF/resin matrix interface and yet, the device was highly sensitive and responsive even after consolidation within a GFRP composite structure under a vacuum pressure and temperature; 2) improved mechanical properties: as the ultimate tensile strength, Young's modulus, strain-to-failure, and strain energy of the smart composite panels were improved, respectively, by ≈40%, ≈10%, and ≈35%; and 3) a very good electrical stability: as no shortage occurred during testing and manufacturing process.

As a result, the empirical findings in this study shed new light on the possibility to develop a new class of smart multifunctional composite structures with improved mechanical properties, and simultaneous EH and vibration damping performances. An implication of this could lead to broad application prospects in electric cars and aircraft (e.g., from fuselage and wings), microair vehicles, composite armor, and cabin noise reduction in an aircraft.

SUPPORTING INFORMATION

Supporting Information is available from the Wiley Online Library at [https://doi.org/10.1002/ente.202000777].

ACKNOWLEDGEMENTS

This research received no specific grant from any funding agency in the public, commercial, or not-for-profit sectors. However, authors would like to acknowledge the assistant and technical supports of many wonderful people at the Department of Aeronautics, Imperial College London, without whom it was not possible to complete this work: Mr. Franco Giammaria, Mr. Joseph Meggyesi, Mr. Roland Hutchins, Mr. Gary Senior, Mr. Keith Wolstenholme, Dr. Frank Gommer, and Mr. Jonathan Cole.

CONFLICT OF INTEREST

The authors declare no conflict of interest.

KEYWORDS

piezoelectric energy harvesting, smart materials, multifunctional composites, poling, characterization

References

[1] Bilal Zaarour, Lei Zhu, Chen Huang, XiangYu Jin, Hadeel Alghafari, Jian Fang, and Tong Lin. A review on piezoelectric fibers and nanowires for energy harvesting. Journal of Industrial Textiles, 0(0):1528083719870197, 2019. https://doi.org/10.1177/1528083719870197.

[2] Jee Siang, MH Lim, and M Salman Leong. Review of vibration-based energy harvesting technology: Mechanism and architectural approach. International Journal of Energy Research, 42(5):1866–1893, 2018. https://doi.org/10.1002/er.3986.

[3] Kai Dong, Xiao Peng, and Zhong Lin Wang. Fiber/fabric-based piezoelectric and triboelectric nanogenerators for flexible/stretchable and wearable electronics and artificial intelligence. Advanced Materials, 32(5):1902549, 2020. https://doi.org/10.1002/adma.201902549.

[4] Guorui Chen, Yongzhong Li, Michael Bick, and Jun Chen. Smart textiles for electricity generation. Chemical Reviews, 120(8):3668–3720, 2020. https://doi.org/10.1021/acs.chemrev.9b00821.

[5] Mengdi Han, Heling Wang, Yiyuan Yang, Cunman Liang, Wubin Bai, Zheng Yan, Haibo Li, Yeguang Xue, Xinlong Wang, Banu Akar, et al. Three-dimensional piezoelectric polymer microsystems for vibrational energy harvesting, robotic interfaces and biomedical implants. Nature Electronics, 2(1):26–35, 2019. https://doi.org/10.1038/s41928-018-0189-7.

[6] Shivam Tiwari, Anupama Gaur, Chandan Kumar, and Pralay Maiti. Enhanced piezoelectric response in nanoclay induced electrospun pvdf nanofibers for energy harvesting. Energy, 171:485–492, 2019. https://doi.org/10.1016/j.energy.2019.01.043.

[7] Abdul-Rahman El-Sayed, Kevin Tai, Mohammad Biglarbegian, and Shohel Mahmud. A survey on recent energy harvesting mechanisms. ECCM17-17th European Conference on Composite Materials, pages 1–5. IEEE, 2016. https://doi.org/10.1109/CCECE.2016.7726698.

[8] Sang Hyun Ji, Yong-Soo Cho, and Ji Sun Yun. Wearable core-shell piezoelectric nanofiber yarns for body movement energy harvesting. Nanomaterials, 9(4):555, 2019. https://doi.org/10.3390/nano9040555.

[9] Hyewon Lee and Jung-Sim Roh. Wearable electromagnetic energy-harvesting textiles based on human walking. Textile Research Journal, 89(13):2532–2541, 2019. https://doi.org/10.1177/0040517518797349.

[10] Fatemeh Mokhtari, Zhenxiang Cheng, Raad Raad, Jiangtao Xi, and Javad Foroughi. Piezofibers to smart textiles: A review on recent advances and future outlook for wearable technology. Journal of Materials Chemistry A, 8(19):9496–9522, 2020. https://doi.org/10.1039/D0TA00227E.

[11] Fatemeh Mokhtari, Javad Foroughi, Tian Zheng, Zhenxiang Cheng, and Geoffrey M Spinks. Triaxial braided piezo fiber energy harvesters for self-powered wearable technologies. Journal of Materials Chemistry A, 7:8245–8257, 2019. https://doi.org/10.1039/C8TA10964H.

[12] Gyeong Ju Song, Jae Yong Cho, Kyung-Bum Kim, Jung Hwan Ahn, Yewon Song, Wonseop Hwang, Seong Do Hong, and Tae Hyun Sung. Development of a pavement block piezoelectric energy harvester for self-powered walkway applications. Applied Energy, 256:113916, 2020. https://doi.org/10.1016/j.apenergy.2019.113916.

[13] Lijun Lu, Wenqing Ding, Jingquan Liu, and Bin Yang. Flexible pvdf based piezoelectric nanogenerators. Nano Energy, page 105251, 2020. https://doi.org/10.1016/j.nanoen.2020.105251.

[14] Lijun Lu, Bin Yang, Yueqi Zhai, and Jingquan Liu. Electrospinning core-sheath piezoelectric microfibers for self-powered stitchable sensor. Nano Energy, 76:104966, 2020. https://doi.org/10.1016/j.nanoen.2020.104966.

[15] Rahul Kumar Singh, Sun Woh Lye, and Jianmin Miao. Measurement of impact characteristics in a string using electrospun pvdf nanofibers strain sensors. Sensors and Actuators A: Physical, 303:111841, 2020. https://doi.org/10.1016/j.sna.2020.111841.

[16] Bojing Shi, Zhuo Liu, Qiang Zheng, Jianping Meng, Han Ouyang, Yang Zou, Dongjie Jiang, Xuecheng Qu, Min Yu, Luming Zhao, et al. Body-integrated self-powered system for wearable and implantable applications. ACS nano, 13(5):6017–6024, 2019. https://doi.org/10.1021/acsnano.9b02233.

[17] Ömer Faruk Ünsal, Ayşe Sezer Hiçyilmaz, Ayten Nur Yüksel Yilmaz, Yasin Altin, İsmail Borazan, and Ayşe Çelik Bedeloğlu. Energy-generating textiles. pages 415–455. Elsevier, 2020. ISBN 978-0-12-820257-9.

[18] Kenji Uchino. Advanced piezoelectric materials: Science and technology. Woodhead Publishing, 2017. ISBN 0081012551.

[19] Vincent L Stuber, Daniella B Deutz, James Bennett, David Cannel, Dago M de Leeuw, Sybrand van der Zwaag, and Pim Groen. Flexible lead-free piezoelectric composite materials for energy harvesting applications. Advanced Materials Technologies, 7(1):177–185, 2019. https://doi.org/10.1002/ente.201800419.

[20] Sibo He, Wen Dong, Yiping Guo, Lin Guan, Hongyuan Xiao, and Hezhou Liu. Piezoelectric thin film on glass fiber fabric with structural hierarchy: An approach to high-performance, superflexible, cost-effective, and large-scale nanogenerators. Nano Energy, 59:745–753, 2019. https://doi.org/10.1016/j.nanoen.2019.03.025.

[21] All Plastics. Pvdf material properties data sheet, 2015. https://www.theplasticshop.co.uk/plastic_technical_data_sheets/pvdf_technical_data_sheet.pdf, Accessed July 23, 2020.

[22] Subash Cherumannil Karumuthil, Sreenidhi Prabha Rajeev, and Soney Varghese. Poly (vinylidene fluoride-trifluoroethylene)-zno nanoparticle composites on a flexible poly (dimethylsiloxane) substrate for energy harvesting. ACS Applied Nano Materials, 2:4350–4357, 2019. https://doi.org/10.1021/acsanm.8b02248.

[23] Nick A Shepelin, Alexey M Glushenkov, Vanessa C Lussini, Phillip J Fox, Greg W Dicinoski, Joseph G Shapter, and Amanda V Ellis. New developments in composites, copolymer technologies and processing techniques for flexible fluoropolymer piezoelectric generators for efficient energy harvesting. Energy & Environmental Science, 12(4):1143–1176, 2019. https://doi.org/10.1039/C8EE03006E.

[24] Abhishek Anand and MC Bhatnagar. Role of vertically aligned and randomly placed zinc oxide (zno) nanorods in pvdf matrix: Used for energy harvesting. Materials Today Energy, 13:293–301, 2019. https://doi.org/10.1016/j.apenergy.2019.113916.

[25] MeasurementSpecialties™. Piezo film sensors technical manual. Technical report, 950 Forge Avenue, Norristown, PA 19403, 2017. https://www.sparkfun.com/datasheets/Sensors/Flex/MSI-techman.pdf.

[26] Navneet Soin, Tahir H Shah, Subhash C Anand, Junfeng Geng, Wiwat Pornwannachai, Pranab Mandal, David Reid, Surbhi Sharma, Ravi L Hadimani, Derman Vatansever Bayramol, et al. Novel "3-d spacer" all fibre piezoelectric textiles for energy harvesting applications. Energy & Environmental Science, 7(5):1670–1679, 2014.

[27] Jaime Martín, Dong Zhao, Thomas Lenz, Ilias Katsouras, Dago M de Leeuw, and Natalie Stingelin. Solid-state-processing of δ-pvdf. Materials Horizons, 4(3):408–414, 2017.

[28] Zhong Li, Jian Wang, Xiao Wang, Qinghao Yang, and Zhicheng Zhang. Ferro-and piezo-electric properties of a poly (vinyl fluoride) film with high ferro- to para-electric phase transition temperature. RSC advances, 5(99):80950–80955, 2015. https://doi.org/10.1039/C5RA15149J.

[29] Sweety Supriya, Lawrence Kumar, and Manoranjan Kar. Optimization of dielectric properties of pvdf–cfo nanocomposites. Polymer Composites, 40(3):1239–1250, 2019. https://doi.org/10.1002/pc.24840.

[30] Jian Fang, Haitao Niu, Hongxia Wang, Xungai Wang, and Tong Lin. Enhanced mechanical energy harvesting using needleless electrospun poly (vinylidene fluoride)

nanofibre webs. Materials, 6(7):2196–2202, 2013. https://doi.org/10.1039/C3EE24230G.

[31] Bilal Zaarour, Lei Zhu, Chen Huang, and Xiangyu Jin. Fabrication of a polyvinylidene fluoride cactus-like nanofiber through one-step electrospinning. RSC advances, 8(74):42353–42360, 2018. https://doi.org/10.1039/C8RA09257E.

[32] Bilal Zaarour, Lei Zhu, and Xiangyu Jin. Direct generation of electrospun branched nanofibers for energy harvesting. Polymers for Advanced Technologies, 2020. https://doi.org/10.1002/pat.4992.

[33] Xin Lu, Hang Qu, and Maksim Skorobogatiy. Piezoelectric micro-and nanostructured fibers fabricated from thermoplastic nanocomposites using a fiber drawing technique: Comparative study and potential applications. ECS Transactions, 86(16), 2018.

[34] Erik Nilsson, Anja Lund, Christian Jonasson, Christer Johansson, and Bengt Hagström. Poling and characterization of piezoelectric polymer fibers for use in textile sensors. Sensors and Actuators A: Physical, 201:477–486, 2013. https://doi.org/10.1016/j.sna.2013.08.011.

[35] Dimitroula Matsouka, Savvas Vassiliadis, and Derman Vatansever Bayramol. Piezoelectric textile fibres for wearable energy harvesting systems. Materials Research Express, 5(6):065508, 2018. https://doi.org/10.1088%2F2053-1591%2Faac928.

[36] Ravi L Hadimani, D Vatansever Bayramol, N Sion, T Shah, Limin Qian, Shaoxin Shi, and E Siores. Continuous production of piezoelectric pvdf fibre for e-textile applications. Smart Materials and structures, 22(7):075017, 2013. https://doi.org/10.1088%2F0964-1726%2F22%2F7%2F075017.

[37] Elias Siores and Magundappa L Ravi Hadimani. Piezoelectric polymer element and production method and apparatus therefor. March 2016; Google Patent; https://patents.google.com/patent/US9287492B2/en.

[38] Kevin Magniez, Andrew Krajewski, Martin Neuenhofer, and Richard Helmer. Effect of drawing on the molecular orientation and polymorphism of melt-spun polyvinylidene fluoride fibers: Toward the development of piezoelectric force sensors. Journal of applied polymer science, 129(5):2699–2706, 2013. https://doi.org/10.1002/app.39001.

[39] Anja Lund, Karin Rundqvist, Erik Nilsson, Liyang Yu, Bengt Hagström, and Christian Müller. Energy harvesting textiles for a rainy day: woven piezoelectrics based on melt-spun pvdf microfibres with a conducting core. npj Flexible Electronics, 2(1):1–9, 2018. https://doi.org/10.1038/s41528-018-0022-4.

[40] Muhammad Maqsood and Gunnar Seide. Novel bicomponent functional fibers with sheath/core configuration containing intumescent flame-retardants for textile applications. Materials, 12(19):3095, 2019. https://doi.org/10.3390/ma12193095.

[41] Yuning Meng, Yang Zhao, Chuangang Hu, Huhu Cheng, Yue Hu, Zhipan Zhang, Gaoquan Shi, and Liangti Qu. All-graphene core-sheath microfibers for all-solid-state, stretchable fibriform supercapacitors and wearable electronic textiles. Advanced materials, 25(16):2326–2331, 2013. https://doi.org/10.1002/adma.201300132.

[42] Seyedalireza Razavi, Lorenzo Iannucci, and Emile Smith Greenhalgh. Piezoelectric pvdf smart fibre for composite applications. ECCM17–17th European Conference on Composite Materials, Munich, Germany, pages 1–8, June 2016. http://hdl.handle.net/10044/1/81073.

[43] Seyedalireza Razavi, Lorenzo Iannucci, and Emile Smith Greenhalgh. Piezoelectric pvdf smart fibre. ECCM17–17th European Conference on Composite Materials, Munich, Germany, pages 1–8. Spiral, 2016. http://hdl.handle.net/10044/1/81084.

[44] Seyedalireza Razavi and Lorenzo Iannucci. Simulation of the braiding process in ls-dyna®. pages 1–8. Detroit, USA, 2018. https://spiral.imperial.ac.uk/bitstream/10044/1/81074/2/LSDYNA_Paper.pdf.

[45] Seyedalireza Razavi. The development of a smart piezo-braid for composite applications. Phd thesis, , Imperial College London, UK, 2020. https://doi.org/10.25560/79779.

[46] Plastics Lenzing. Lenzing lenofil pvdf multifilament yarn, 2020. https://www.lenzing-plastics.com/en/, Accessed August 13, 2020.

[47] Syscom Advanced Materials. Amberstrand166™, 2015. http://www.metalcladfibers.com/amberstrand, Accessed May 10, 2020.

[48] Syscom Advanced Materials. Liberator 40™, 2015. http://www.metalcladfibers.com/liberator, Accessed May 10, 2020.

[49] Swicofil AG. Polyamide 6.6 conductive yarns and fibers, 2018. https://www.swicofil.com/commerce/products, Accessed July 20, 2020.

[50] RS Components Ltd. Block single core 0.4 mm diameter copper wire, 2020. https://uk.rs-online.com/web/p/copper-wire/3377050/, Accessed July 23, 2020.

[51] Standard ASTM. D1577-01 standard test methods for linear density of textile fibers. Technical report, American Society for Testing Materials, West Conshohocken, PA; ASTM International, 2001. https://doi.org/10.1520/D1577-01.

[52] Standard ASTM. D2256/d2256m-10 standard test method for tensile properties of yarns by the single-strand method. Technical report, American Society for Testing Materials, West Conshohocken, PA; ASTM International, 2015. https://doi.org/10.1520/D2256_D2256M-10R15.

[53] Standard ASTM. D7269/d7269m-11 standard test methods for tensile testing of aramid yarns. Technical report, American Society for Testing Materials, West Conshohocken, PA; ASTM International, 2011. https://doi.org/10.1520/D7269_D7269M-11.

[54] Bilal Zaarour, Lei Zhu, Chen Huang, and Xiangyu Jin. Enhanced piezoelectric properties of randomly oriented and aligned electrospun pvdf fibers by regulating the surface morphology. Journal of Applied Polymer Science, 136(6):47049, 2019.

[55] Liuxia Ruan, Xiannian Yao, Yufang Chang, Lianqun Zhou, Gaowu Qin, and Xianmin Zhang. Properties and applications of the β phase poly (vinylidene fluoride). Polymers, 10(13):228, 2018. https://doi.org/10.3390/polym10030228.

[56] Bilal Zaarour, Lei Zhu, and Xiangyu Jin. Controlling the surface structure, mechanical properties, crystallinity, and piezoelectric properties of electrospun pvdf nanofibers by maneuvering molecular weight. Soft Materials, 17(2):181–189, 2019. https://doi.org/10.1080/1539445X.2019.1582542.

[57] Anja Lund, Karin Rundqvist, Erik Nilsson, Liyang Yu, Bengt Hagström, and Christian Müller. Poling-free spinning process of manufacturing piezoelectric yarns for textile applications. Materials & Design, 179:107889, 2019. https://doi.org/10.1016/j.matdes.2019.107889.

[58] V Sencadas, S Lanceros-Méndez, and JF Mano. Characterization of poled and non-poled β-pvdf films using thermal analysis techniques. Thermochimica acta, 424(1–2):201–207, 2004. https://doi.org/10.1016/j.tca.2004.06.006.

[59] IO Pariy, AA Ivanova, VV Shvartsman, DC Lupascu, GB Sukhorukov, MA Surmeneva, and RA Surmenev. Poling and annealing of piezoelectric poly (vinylidene fluoride) micropillar arrays. Materials Chemistry and Physics, 239:122035, 2020. https://doi.org/10.1016/j.matchemphys.2019.122035.

[60] Mandakini Sharma, Jitendra Kumar Quamara, and Anurag Gaur. Behaviour of multiphase pvdf in (1- x) pvdf/(x) batio 3 nanocomposite films: structural, optical, dielectric and ferroelectric properties. Journal of Materials Science: Materials in Electronics, 29:10875–10884, 2018. https://doi.org/10.1007/s10854-018-9163-4.

[61] Xiaomei Cai, Tingping Lei, Daoheng Sun, and Liwei Lin. A critical analysis of the α, β and γ phases in poly (vinylidene fluoride) using ftir. RSC advances, 258:15382–15389, 2017. https://doi.org/10.1039/C7RA01267E.

[62] Measurement Specialties$_{TM}$ The ETE Connectivitiy. Piezo spiral wrapped coaxial cable, 2011. https://manualzz.com/doc/9646527/piezo-spiral-wrapped-coaxial-cable.

[63] Heiji Kawai. The piezoelectricity of poly (vinylidene fluoride. Japanese journal of applied physics, 8(7):975, 1969. https://doi.org/10.1143%2Fjjap.8.975.

[64] Standard ASTM. D7264/d7264m-15 standard test method for flexural properties of polymer matrix composite materials. Technical report, West Conshohocken, PA; ASTM International.

[65] Measurement Specialties$_{TM}$ The ETE Connectivitiy. Piezo film lab amplifier, 2020. https://www.te.com/commerce/DocumentDelivery/DDEController?Action=showdoc&DocId=Data+Sheet%7FPiezo_Film_Lab_Amplifier%7FA1%7Fpdf%7FEnglish%7FENG_DS_Piezo_Film_Lab_Amplifier_A1.pdf%7FCAT-PFS0015.

[66] Tobias Wehrkamp-Richter, Roland Hinterhoelzl, and Silvestre Pinho. Damage and failure of triaxial braided composites under multi-axial stress states. Composites Science and Technology, 150:32–44, 07 2017.

[67] Henry A Sodano, Daniel J Inman, and Gyuhae Park. Comparison of piezoelectric energy harvesting devices for recharging batteries. Journal of intelligent material systems and structures, 16(10):799–807, 2005. https://doi.org/10.1177/1045389X05056681.

[68] Henry A Sodano, Daniel J Inman, and Gyuhae Park. Generation and storage of electricity from power harvesting devices. Journal of intelligent material systems and

structures, 16(1):67–75, 2005. https://doi.org/10.1177/1045389X05047210.

[69] Standard test methods for linear density of textile fibers. Standard, American Society for Testing Materials, West Conshohocken, United States, 2017. https://doi.org/10.1520/D3039_D3039M-17.

[70] Xia Liu, Jing Ma, Xiaoming Wu, Liwei Lin, and Xiaohong Wang. Polymeric nanofibers with ultrahigh piezoelectricity via self-orientation of nanocrystals. ACS nano, 11(2):1901–1910, 2017. https://doi.org/10.1021/acsnano.6b07961.

[71] Zhao Guan, Zhen-Zheng Jiang, Bo-Bo Tian, Yi-Ping Zhu, Ping-Hua Xiang, Ni Zhong, Chun-Gang Duan, and Jun-Hao Chu. Identifying intrinsic ferroelectricity of thin film with piezoresponse force microscopy. AIP Advances, 7(9):095116, 2017. https://doi.org/10.1063/1.4999199.

[72] Khrissy Aracélly Reis Medeiros, Carlos Roberto Hall Barbosa, José Roberto Moraes d'Almeida, Alexandre Sant'Anna Ribeiro, and Igor Braga de Paula. Flowmeter based on a piezoelectric pvdf tube. Measurement, 138:368–378, 2019. https://doi.org/10.1016/j.measurement.2019.02.059.

[73] Vitor Sencadas, M Vitor Moreira, Senentxu Lanceros-Méndez, António Sergio Pouzada, and Rinaldo Gregório Filho. α-to β transformation on pvdf films obtained by uniaxial stretch. Materials science forum, 514:872–876, 2006. https://doi.org/10.4028/www.scientific.net/MSF.514-516.872.

[74] Ganji Zhong, Lifeng Zhang, Run Su, Ke Wang, Hao Fong, and Lei Zhu. Understanding polymorphism formation in electrospun fibers of immiscible poly (vinylidene fluoride) blends. Polymer, 52:2228–2237, 2011. https://doi.org/10.1016/j.polymer.2011.03.024.

[75] Suresha K Mahadeva, John Berring, Konrad Walus, and Boris Stoeber. Effect of poling time and grid voltage on phase transition and piezoelectricity of poly (vinyledene fluoride) thin films using corona poling. Journal of Physics D: Applied Physics, 46(28):285305, 2013. https://doi.org/10.1088%2F0022-3727%2F46%2F28%2F285305.